Texture and magnetic anisotropy of $YBa_2Cu_3O_{7-x}$ film on MgO substrate

H. Sanchez Cornejo[1], L. De Los Santos Valladares[2,3,*] (ID), C. H. W. Barnes[3],
N. O. Moreno[4], and A. Bustamante Domínguez[1]

[1] *Laboratorio de Cerámicos y Nanomateriales, Facultad de Ciencias Físicas, Universidad Nacional Mayor de San Marcos, Ap. Postal 14-0149, Lima 14, Perú*

[2] *School of Materials Science and Engineering, Northeastern University, No 11, Lane 3, Wenhua Road, Heping District, Shenyang 110819, Liaoning, People's Republic of China*

[3] *Cavendish Laboratory, Department of Physics, University of Cambridge, J. J. Thomson Ave., Cambridge CB3 0HE, UK*

[4] *Departamento de Física, Universidade Federal de Sergipe, São Cristóvão, SE 49100-000, Brazil*

ABSTRACT

The texture and magnetic anisotropy of a $YBa_2Cu_3O_{7-x}$ (YBCO) film growth onto a MgO substrate are analyzed in order to understand the relation between them. X-ray diffraction shows the presence of the (00*l*) reflections from the YBCO layer with a grain's fraction value 98%. Rocking Curves (RC) measurements reveal an out-of-plane texture with a full width at the half maximum of 0.81°, revealing a high uniaxial texture in the YBCO film. The temperature dependence of the susceptibility measurements obtained under many applied fields along H_{ext} ||*c*-axis and H_{ext}||*ab*-plane reveals strong relationship between the uniaxial texture and the magnetic anisotropy, confirming the high ordering of the CuO_2 superconducting planes. In addition, the critical current density values are obtained from the hysteresis loops and compared to similar YBCO films with uniaxial and biaxial texture reported elsewhere.

1 Introduction

The importance of electrical transport properties in superconducting materials has led to an extensive experimental research and development of highly textured layers of $YBa_2Cu_3O_{7-\delta}$ (YBCO) on a variety of substrates [1]. Due to the anisotropy of YBCO, it is necessary to use epitaxial layers with a biaxial textured YBCO (i.e., with good out-of-plane and in-plane texture) to achieve critical current densities higher than 10^6 A/cm^2 at 77 K [2].

In thin films, texture is referred to the relative ordering of crystallites to a particular direction of growth, called texture axis [2, 3]. Texture can be uniaxial or biaxial, depending on the prevalence of one or two directions of arrangement of the superconducting grains, respectively. Quantifying the degree of texture in YBCO layers is commonly achieved by various experimental techniques, such as

Address correspondence to E-mail: luisdv@mail.neu.edu.cn; ld301@cam.ac.uk

X-ray diffraction (pole figure (φ and ψ-scans) and ω-scan), Raman spectroscopy, optical techniques, transmission electron microscopy (TEM), and scanning electron microscopy (SEM). The degree of texture out-of-plane direction is estimated by θ-2θ and ω-scans, while a measure of the degree of texture in the plane can be achieved by means of a measurement of the figure pole or φ-scan [3].

In contrast to uniaxial texture, high degree of biaxial crystalline texture provides high critical current densities in YBCO films [2, 4]. In addition, understanding the processes governing the formation of c-axis and a-axis crystals is very important since the formation of 90° grain boundaries may strongly deteriorate the critical currents [5].

To achieve the epitaxial growth along the c-axis (i.e., uniaxial texture), the crystal lattice of the substrate must match with that of YBCO, permitting a little difference between them. If the lattice constant of the substrate differs a lot from that of YBCO, the epitaxial growth is not achieved [6] or results in a low amount of grains oriented in the textured direction [2]. Much investigation have been performed on both, uniaxial and biaxial, YBCO films grown onto different substrates such as $LaAlO_3$ ($a_{LaAlO_3} \sim 3.8 \mathring{A}$) and $SrTiO_3$ ($a_{SrTiO_3} \sim 3.9 \mathring{A}$) because their cell parameters are quite similar to that for YBCO ($a_{YBCO} \sim 3.8 \mathring{A}$) [6]. Those studies focus on the fabrication, texture and characterization by different physical and chemical techniques of the YBCO film [7–9] without paying much attention to the magnetic anisotropy properties [10]. The magnetic anisotropy on YBCO films have been only reported as complementary information to other characterization techniques rather than extensive analysis attempting to relate it to the texture [11–14].

On the other hand, uniaxial and biaxial YBCO layers can be also deposited onto other substrates with large cell parameters, such as MgO ($a_{MgO} \sim 4.1 \mathring{A}$) [15–22]. No studies have been reported about the magnetic anisotropy of uniaxial or biaxial YBCO films grown onto MgO single-crystal substrate. Such studies are important since well-oriented crystals achieve a high magnetic anisotropy and thus, high current density values. This is important since high J_C values are crucial for potential applications of the YBCO in electrical devices.

In this work, we analyze the uniaxial texture of YBCO onto MgO substrates and the magnetic anisotropy obtained under many different external magnetic fields applied parallel and perpendicular to the plane of the substrate and at different temperatures. We found that uniaxial texture ordering influences in the magnetic anisotropy of the YBCO film. In addition, the obtained critical current density is compared to those ones reported elsewhere for other similar uniaxial and biaxial YBCO films.

2 Experimental section

A YBCO thin film was obtained from the CERACO Ceramic Coating GmBH Inc. Germany (MgO X260314B E-Type), which was deposited on an MgO substrate by the Sputtering technique. This sample is sold by CERACO suggesting application on low-temperature electronics, multilayers and submicron structures. The sample has a size of 10×10 mm^2. The crystallization of the sample was studied by X-ray diffraction (XRD). The data were collected from 8 to 80° (0.01° step) using a powder universal diffractometer Bruker D8 with Cu K$_{\alpha 1}$ radiation (λ =1.54056 Å). The texture was analyzed by Rocking Curves measurements around the reflection (005) 2Θ = 38.72° with 0.02° (ω) step and time step 6 s by 15° to 23 intervals. The crystallite size was estimated from the basic Scherrer's formula, neglecting peak broadening caused by residual stresses in the films [23]. D is the average crystallite size, λ is the wavelength of the applied X-ray ($\lambda_{Cu-K\alpha 1}$ = 0.154056 nm), θ_{hkl} is the Bragg's angle, β_{hkl} is the width of the X-ray peak on the 2Θ axis, which were easily found by measuring the full width at the half maximum (FWHM) of the reflection and K is the so-called Scherrer Constant. K depends of the crystallite shape and the size distribution, indices of the diffraction line, and the actual definition used for β whether FWHM or integral breadth [24]. K can have values anywhere from 0.62 and 2.08. In this paper, K = 0.916 was used. Further, microstrain in the crystallite or nanocrystal also affects the width β, which needs to be considered in an accurate analysis. Spatial fluctuations in the alloy composition can also affect the width. In this work, the calculated values of D represent estimates.

$$D = \frac{K\lambda}{\beta_{hkl}\cos\theta_{hkl}} \tag{1}$$

The alignment of the magnetic moments was studied as a function of temperature under different

applied magnetic fields in a DC Magnetic Property Measurement System (DC-MPMS-SQUID) from Quantum Design. The data were collected in Zero Field Cooling (ZFC) and Field Cooling (FC) modes. The roughness was examined using an AFM (atomic force microscopy) Nanoscope Dimension 3100 from Digital Instruments in tapping mode. The AFM data were analyzed with the help of the WSxM 3.1 software [25]. For the TEM measurements, the sample was coated with a Pt protective layer, then milled and thinned with a focused ion beam (FIB) in a dual-beam Quanta 3D apparatus (Philips). The interface was inspected in a Tecnai 20 (Philips) microscope, with a 200 keV beam generated by a tungsten source.

3 Results and discussion

Figure 1 shows the XRD (in normal and at logarithmical scale) of the YBCO film on the MgO substrate. The presence of the peaks (002), (003), (004), (005), (006) and (007) reveals epitaxial growth in the c-direction or texture axis. The three close strong reflections at 42.94°, 42.97° and 43.07° correspond to the MgO substrate. The Y_2BaCuO_5 (Y211) and CuO are also detected as secondary phases. The Y211 phase (PDF card 78-1719 [26]) is detected by the reflections around 34.41°, 35.48° and 59.92°. The CuO phase is

observed in relative minor amount with reflections around 65.91° and 72.63°.

The texture of the formed film was analyzed from the fraction of c-axis orientation, fc, using Eq. (2) [2].

$$\frac{I^{005}}{I^{200}} = \frac{f_c \cdot I_{stand}^{005}}{(1 - f_c) I_{stand}^{200}} \tag{2}$$

where I_{stand} is the standard intensity obtained for randomly oriented samples (PDF card 40-159 [26]). We obtain $f_c = 0.98$. Therefore, 98% of the superconductor phase in the film followed the preferential orientation given by the substrate. The crystallite size value of 56 nm was calculated using Eq. (1).

To study the quality of the out-of-plane texture, rocking curves measurements are performed around the (005) reflection (see inset Fig. 1). This reflection was chosen because its intensity is higher than the other (00l) reflections and also because its position in XRD plot (around $2\theta = 38.72°$) is far away from any other reflection from the substrate, thus preventing the reflection´s texture will add to the final measure.

The full width at half maximum (FWHM) value of the Rocking curve (RC) provides information about the degree of inclination of the c-axes of the superconducting grains with respect to the normal of the plane substrate [2]. The RC measurement allows us to observe one region with out-of-plane texture for the
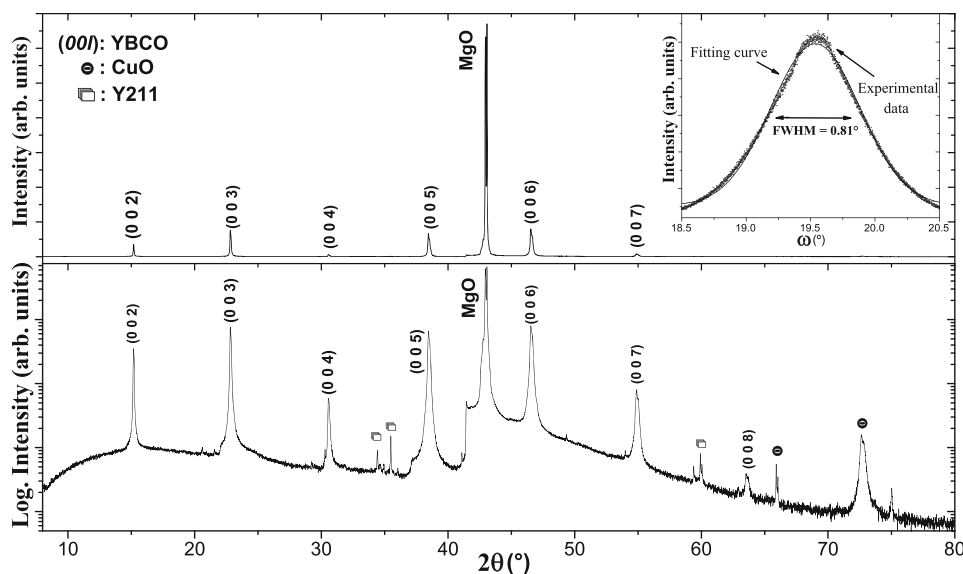

Fig. 1 XRD pattern of the YBCO film grown on MgO substrate. Top: the normal intensity axis is in arbitrary units and bottom: XRD in semi-logarithmical scale. The presence of the (00l) reflections corresponding to YBCO indicates crystallite growth in the c-direction. In addition to the YBCO phase, small reflections corresponding to the phases CuO (unreacted) and Y_2BaCuO_5 (secondary) were also detected. Inset: rocking curve around (005) YBCO reflection

sample where the obtained value is 0.81° of FWHM ($\Delta\omega$).

Figure 2 shows the morphology of the sample. Figure 2a shows the optical microscopy image (at 100×) of the surface of the sample. Despite some impurity grains on the surface, the image suggests a compact film. Figure 2b shows the topography of the surface of the YBCO film over $1 \times 1 \ \mu m^2$ area obtained by AFM. The inset plot shows the profile obtained over the dashed line drown on the AFM image. For the roughness analysis, the average roughness (R_a) [27] was computed from the arithmetic mean of the deviations in height from the image mean value (Eq. 3).

$$R_a = \frac{1}{N}\sum_{i=1}^{N}|Z_i - \overline{Z}|$$ (3)

Moreover, the RMS (root-mean-square-roughness) [27] is defined as the square root of the mean value of the squares distance of the points from the image mean value and is calculated by Eq. (4). The maximum P-V (peak-to-valley) is obtained from the AFM morphology analysis.

$$RMS = \sqrt{\frac{1}{N}\sum_{i=1}^{N}(Z_i - \bar{Z})^2}$$ (4)

The high roughness morphology of the surface is caused by the formation of a compacted film, according to the first look observed in Fig. 2b. The calculated roughness parameters for the AFM surface profiles shown in Fig S1 (supporting information) are listed in Table 1. Figure 2c shows the cross-sectional view of the film with a Pt layer used for protecting, as mentioned in the experimental section. This image suggests that the film is compact. It also suggests that the film has been grown in a layer-by-layer fashion. This is confirmed by the high-resolution TEM image of the YBCO film (Fig. 2d), which reveals the epitaxial growth of the YBCO film following the same order of the substrate. It also shows crystallites of the YBCO with interplanar distance 2.9 Å corresponding to the (004) reflection, in agreement to the XRD analysis discussed above. The YBCO/MgO (film/substrate) interphase is indicated with a dashed line.

Figure 3 shows the temperature dependence of the susceptibility of the sample in the superconducting
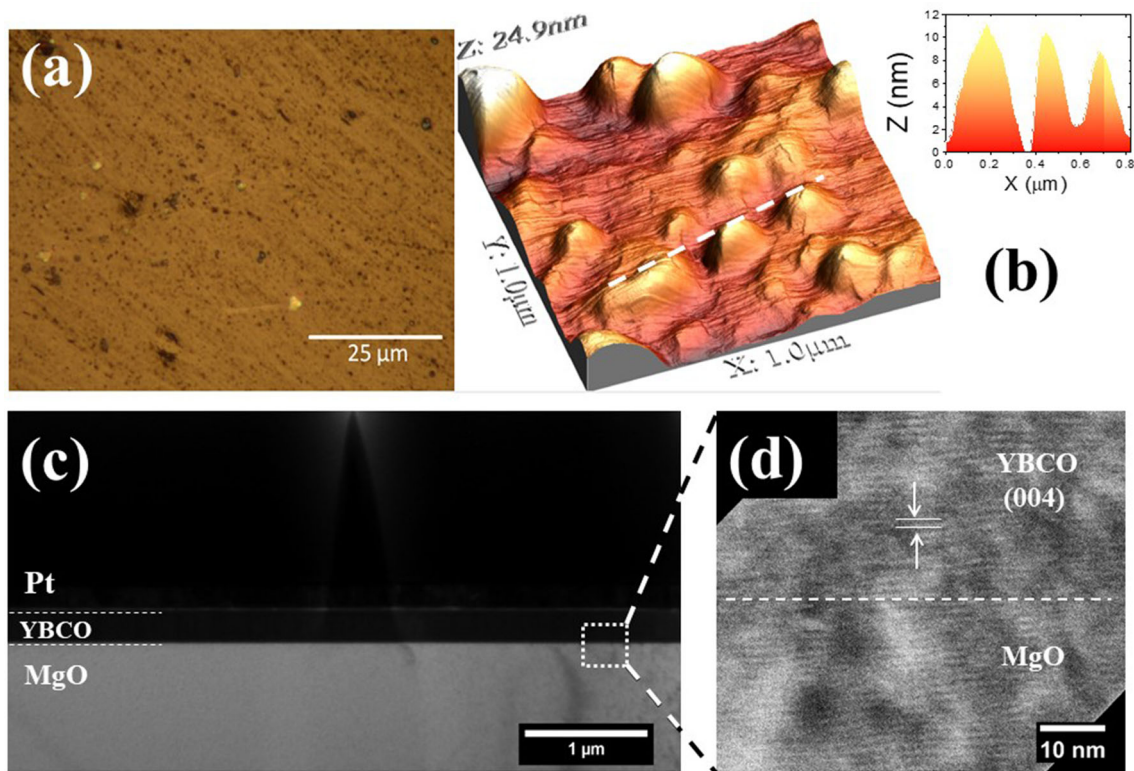

Fig. 2 Morphology of a YBCO film on MgO substrate. **a** Optical microscope image of the surface of the sample, **b** surface topography obtained by AFM and the profile obtained over the dashed line, **c** cross-sectional TEM image and **d** HR-TEM image

Table 1 Roughness parameters of the YBCO film grown on MgO substrate.

Type of roughness	$50 \times 50 \ \mu m^2$	$5 \times 5 \ \mu m^2$	$1 \times 1 \ \mu m^2$
Average roughness (R_a)	9.9 nm	4.4 nm	2.9 nm
Root-mean-square-roughness(RMS)	14.2 nm	7.7 nm	4.4 nm
Peak-to-valley (P-V)	130 nm	131.1 nm	42.4 nm
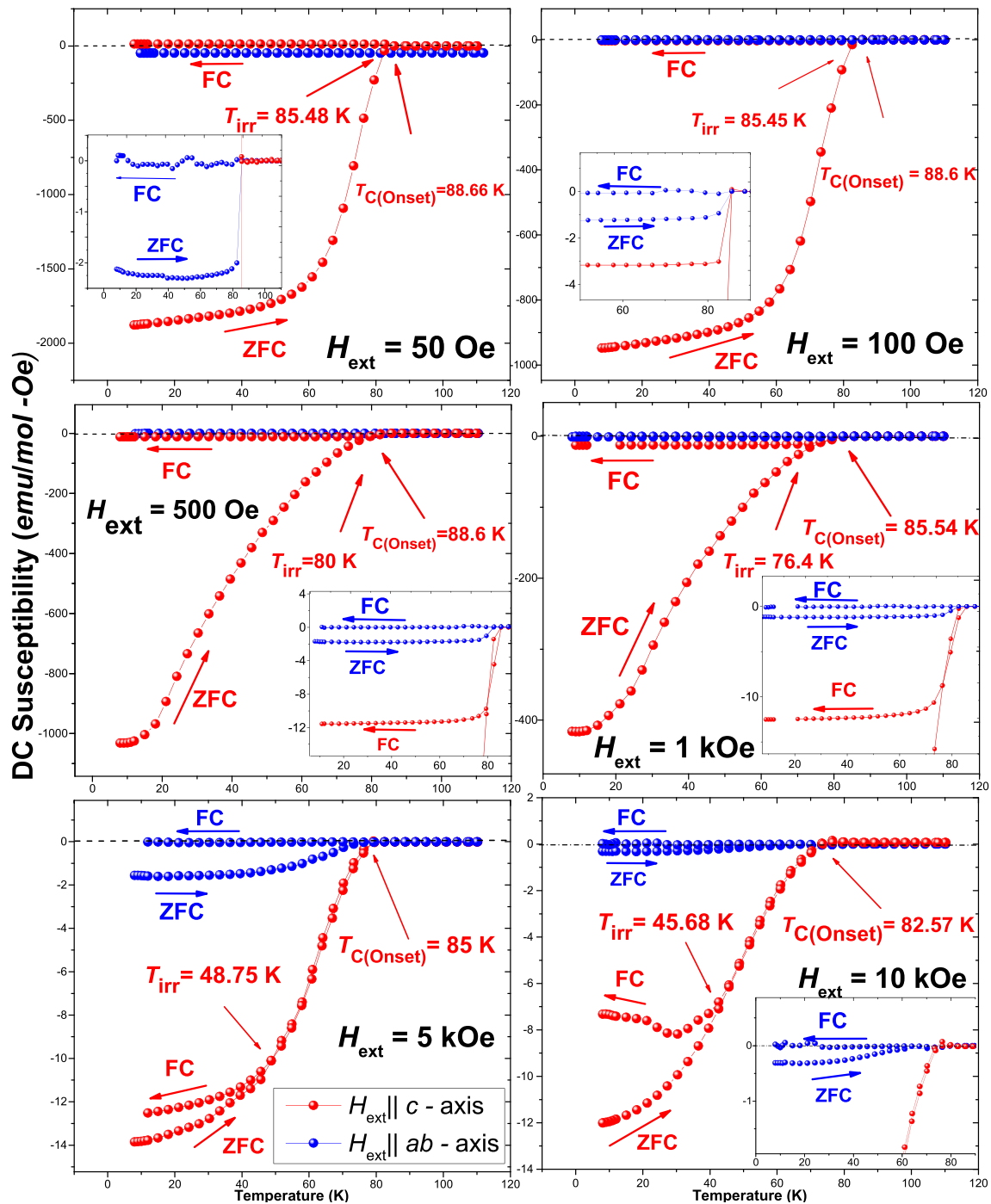
Fig. 3 Temperature dependence of the susceptibility of the YBCO sample grown on MgO substrate obtained under different applied magnetic fields parallel ($H_{ext} \parallel ab$-plane) and perpendicular ($H_{ext} \parallel$ c-axis) to the plane of the substrate. It is observed a strong anisotropy behavior

state and measured under applied magnetic fields 50, 100, 500, 1000, 5000 and 10000 Oe. The anisotropy behavior of the magnetization in the YBCO film was detected by applying the external magnetic fields parallel and perpendicular to the plane of the substrate. According to the figure, the sample becomes diamagnetic (indicating the Meissner effect, typical from superconductors) from the onset temperature $T_{C(onset)} \approx 88,6$ K under H_{ext} =50 Oe. This temperature is dependent of the magnitude and direction of the applied magnetic field. The point from which the ZFC and FC loops diverge defines the irreversibility temperature (T_{irr}) and it also depends on the magnitude of the external magnetic field [1]. In this work $T_{irr} \approx 80$ K under the applied magnetic field of 500 Oe. The critical temperatures were estimated from the maximum inflexion points of the derivative of the loops (see Fig. 4). They are 88, 87.8, 86, 85.7, 84 and 79.2 K under the applied magnetic fields of 50, 100, 500, 1000, 5000 and 10000 Oe respectively. From the same way, irreversibility temperatures values 88.66, 85.45, 80, 76.4, 48.75 and 45.68 K were estimated from the χ(T) curves.

Note that for all the applied magnetic fields, the ZFC and FC susceptibilities signals are higher when H_{ext} is applied parallel (i.e., along the CuO$_2$ superconducting planes) than perpendicular to the c-axis. Since the rocking curve above shows good out-of-plane texture with respect to the c-axis, it is understood that the low mosaicity obtained for the YBCO grains does contribute significantly to the intrinsic strong anisotropy of the YBCO.

Figure 4a and b shows the first derivate of the χ(T) loops. The full width at the half maximum (FWHM) is related to the transition interval and therefore to the texture and homogeneity of the stoichiometric of the sample [12]. The existence of stoichiometric inhomogeneities in the film results in the presence of some domains with different magnetic anisotropy. These domains are tilted around 0.81° respecting to the c-axis for all cases. The FWHM values increase with the applied magnetic field. It is found that the FWHM values are higher when H_{ext} is applied along the c-axis than along the a,b-plane. This increase in the width of the superconducting transition might be related to the secondary phases found by the XRD and TEM above. They might create a paramagnetic contribution in the χ(T) loops, specially at the low-temperature region. Such signal screens the diamagnetic one from the YBCO superconductor,

increasing the χ and the FWHM values. Thus, the magnetic anisotropy behavior in the present uniaxial texture YBCO films is better analyzed at low applied fields and temperatures close to T_C.

The applied field dependences of the magnetization loops are shown in Fig. 5a. They were measured in the temperature range 10-70 K, revealing hysteresis loops typical from the YBCO superconductor. The dissipation energy is represented by the internal area for each cycle and decreases as the temperature approaches to T_C. Using the Bean critical state model [28], the critical current density J_C can be calculated from the width ΔM of $M(H)$ loops, according to Eq. (5) [29], where $\Delta M = M^- - M^+$, the unit of ΔM is emu/cm^3, and w, l are the width and length of the sample measured in cm ($w<l$), respectively.

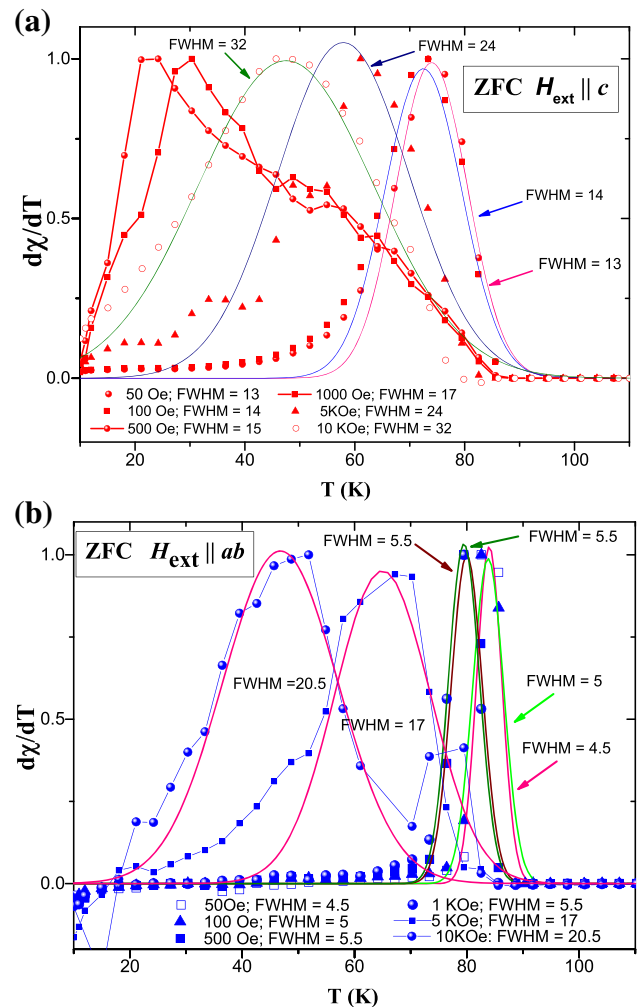**Fig. 4** First derivate of the ZFC curves from the χ(T) loops obtained under different applied magnetic fields along: **a** the c-axis ($H_{ext} \parallel$ c-axis) and **b** the ab-plane ($H_{ext} \parallel$ ab-plane)
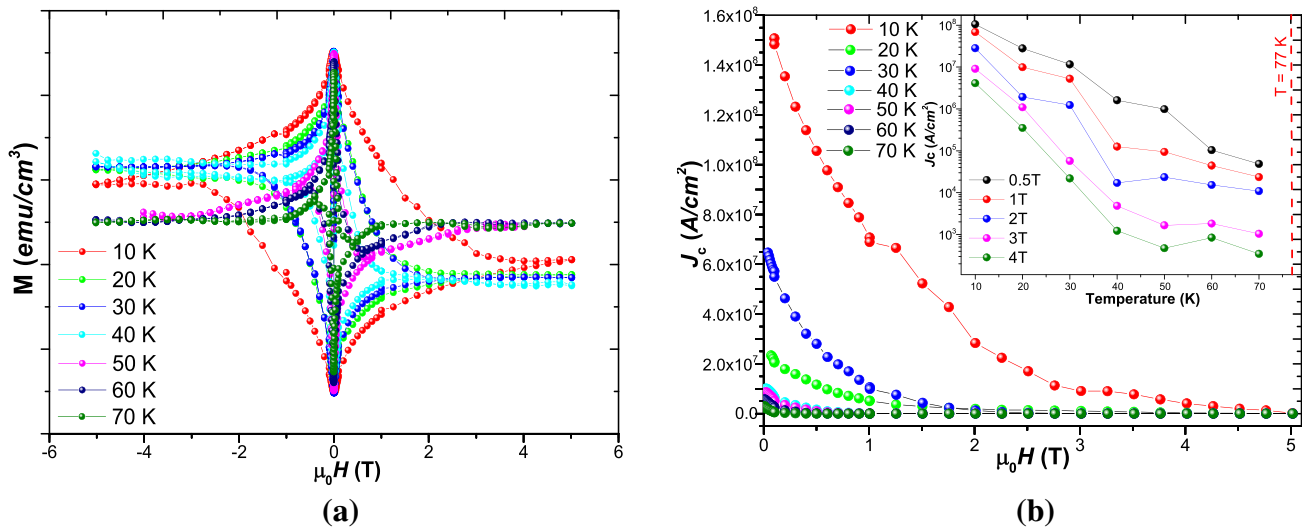
Fig. 5 a Magnetization hysteresis loops of the YBCO/MgO film measured at different temperatures. **b** Field dependence of the J_C, obtained from the Bean critical state model. Inset: $J_C(T)$ curves

Table 2 Characteristics of YBCO films grown on MgO substrates reported in the literature

Texture	Thickness	Characteristics	T_{growth}	J_C (at 77 K, in self-field)	Reference
Uniaxial	200 nm	Reactive thermal co-evaporation technique	760 °C	2.4×10^6 A/cm^2	[15]
	200 nm	Co-evaporation and lithography process	760 °C	2.2×10^6 A/cm^2	[15]
	170 nm	Pulsed laser deposition technique	750 °C	1.2×10^7 A/cm^2	[16]
	200 nm	Excimer laser ablation method. c-axis oriented	Not reported	5×10^5 A/cm^2	[17]
	200 nm	Laser ablation deposition, FWHM =0.3°	670 °C	$3.4–6 \times 10^6$ A/cm^2	[20]
	2 μm	Sputtering technique, Multilayer buffer c-axis orientation	850 °C	5×10^6 A/cm^2	[21]
Biaxial	400 nm	Inclined substrate deposition technique	700–800 °C	1.2×10^6 A/cm^2	[13]
	4.8 μm	MOCVD reactor, IBAD MgO substrate	Not reported	15.11×10^6 A/cm^2 (at 30 K, 3T)	[14]
	100 nm	YBCO/MgO/NiO/Ni tape, Rocking curve FWHM = 2°	700–750 °C	$0.4–0.6 \times 10^5$ A/cm^2	[18]
	1.5 μm	IBAD MgO, FWHM=2.2°	Not reported	2×10^6 A/cm^2	[19]
	1.6 μm	IBAD MgO, FWHM = 1.3°	Not reported	1.1×10^6 A/cm^2	[22]
	150 nm	Using bicrystal MgO substrate with 24° tilt angle by pulsed laser deposition	800 °C	1×10^7 A/cm^2	[31]
	100–140 nm	MOCVD technique	820 °C	$J_C > 10^6$ A/cm^2	[32]

$$J_C = \left[\frac{20\Delta M}{w\left(1 - \frac{w}{3l}\right)} \right] \quad (5)$$

where M^+ and M^- are the magnetization branches in the fully penetrated state for decreasing and increasing applied fields, respectively.

Figure 5b shows the critical current density $J_C(H)$ curves indirectly obtained from the $M(H)$. The estimated $J_C(T)$ is also shown in the inset of the figure,

where the magnitude order J_C (at $\mu_0 H = 0T$, 77K) $\sim 10^5 A/cm^2$ is estimated. Table 2 lists the J_C values and other characteristics for uniaxial and biaxial YBCO films grown onto MgO reported in the literate. Note that J_C values lower than $10^6 A/cm^2$ are reported for uniaxial texture, whereas higher values than $10^6 A/cm^2$ are reported for biaxial texture YBCO films. Considering that J_C values improve with the ordering of the CuO_2

superconducting planes, and biaxial YBCO films present the higher J_C values than uniaxial YBCO films. Thus, the magnetic anisotropy depends on the epitaxy and texture of the YBCO films. YBCO films with high J_C values grown on other substrates different than MgO or using adhesion promoters [30] are out of the scope of this work; nonetheless some of them are listed in Table S1.

Note that in addition to texture, the thickness of the film is also an important parameter. YBCO films with smaller thickness present higher J_C values. This is because J_C is inversely proportional to the volume of the film (Eq. (5)). For example, the $J_C = 1.2 \times 10^7$ Acm^{-2} reported in Ref. [16] for a uniaxial YBCO/MgO film with thickness of 170 nm is higher than that $J_C = 1.2 \times 10^6$ A/cm^2 reported for a biaxial film with 400 nm thickness reported in Ref. [13]. Therefore, the thickness (and thus the volume) influences more than the texture in the J_C values of the YBCO films. YBCO films with high J_C values could be achieved by combining both parameters.

4 Conclusions

The texture and magnetic anisotropy of a superconducting YBCO film grown onto MgO substrate have been analyzed. X-ray diffraction reveals that the crystallites of the sample are oriented along $(00l)$ indicating a uniaxial texture growth of the film in the c-direction. This is confirmed by the cross-sectional TEM measurements. Rocking curves over the (005) reflection of this film can be fitted with one Gaussian function suggesting that the sample consists of a uniform layer deviated $\sim 0.81°$ from the c-axis, confirming the high-quality uniaxial alignment in the film. AFM measurements revealed an average roughness $R_a = 9.9363$ nm around the nanometer scale, that is, a smooth surface. Magnetic measurements estimate the superconducting transition temperature $T_{c(onset)} \approx 88,6$ K under $H_{ext} = 50$ Oe. Despite the good uniaxial texture of the sample, the $\chi(T)$ curves measured under different $H_{ext}||c$-axis and $H_{ext}||ab$-plane show that the small amount of secondary phases has a contribution distorting the superconducting diamagnetic signal. This contribution increases with applied magnetic field as it is suggested by the increase of the FWHM of the first derivate of the χ (T) curves. Thus, the relationship between the texture and magnetic anisotropy is better

analyzed at low applied fields. Under these conditions, the $\chi(T)$ signals reveal strong relationship between the uniaxial texture and the magnetic anisotropy and confirming high ordering of the CuO_2 superconducting planes along the c-axis in the film. In addition, from the $M(H)$ hysteresis loops obtained under $H_{ext}||c$-axis and at different temperatures, the current densities were calculated. A critical current density $J_C(at\mu_0H = 0T, 77K) \sim 10^5 A/cm^2$ is estimated, which is in the same order value reported in the literature for typical YBCO uniaxial textured films. It is expected that a biaxially textured film would present a higher ordering of the CuO_2 planes and thus higher J_C.

Acknowledgements

Electronic supplementary material: The online version of this article (https://doi.org/10.1007/s10854-020-04623-w) contains supplementary material, which is available to authorized users.

References

1. A. Bustamante Domínguez, L. León Félix, J. Garcia, J. Flores Santibañez, L. De Los Santos Valladares, J.C. González, A. Osorio Anaya, M. Pillaca. Epitaxial growth of $YBa_2Cu_3O_7$ films onto $LaAlO_3$ (100) by using oxalates, Phys. Proc. **36**, 526–531 (2012).

2. T. Puig; P. M. Anna; N. Mestres; H. S. Van; F. Alsina; J. C. González; et al. Texture analysis of coated conductors by micro-raman and synchrotron x-ray diffraction, Mat. Res. Soc. Symp. 659, II5.6.1. (2001).

3. X. Obradors, T. Puig, A. Pomar, F. Sandiumenge, S. Piñol, N. Mestres, O. Castaño, M. Coll, A. Cavallaro, A. Palau, J. Gázquez, J.C. González, J. Gutierrez, N. Romá, S. Ricart, J.M. Moretó, M.D. Rossell, G. van Tendeloo, Chemical solution deposition: a path towards low cost coated conductors. Supercond. Sci. Technol. **17**, 1055–1064 (2004)

4. D.T. Verebelyi, D.F. Christen, R. Feenstra, C. Cantoni, A. Goyal, D.F. Lee, M. Paranthaman, P.N. Arendt, D.F. DePaula, J.R. Groves, C. Prouteau, Low angle grain boundary transport in $YBa_2Cu_3O_{7-\delta}$ coated conductors. Appl. Phys. Lett. **76**, 1755 (2000)

5. G. Kästner, C. Schäfer, St.- Senz, T.- Kaiser, H.A. Hein, M. Lorenz, H. Hochmuth, D. Hesse, Supercond. Sci. Technol. **12**, 3661 (1999)

6. L. De Los Santos Valladares, J.C. González, A. Bustamante Domínguez, A.M. Osorio Anaya, H. Sanchez Cornejo, S. Holmes, J. Albino Aguiar, C.H.W. Barnes, A fluorine-free oxalate route for the chemical solution deposition of $YBa_2Cu_3O_7$ films in Superconductors, edited by Alexander Gabovich, ISBN 978-953-51-4163-1. Intech, Chapter 3, 2015, pp 35-53.

7. X. Tang. Development of a fluorine-free chemical solution deposition route for rare-earth cuprate superconducting tapes and its application to reel-to-reel processing. Doctoral thesis. Technical University of Denmark, Denmark.

8. J. C. Gonzalez. Coated conductors and chemical solution growth of YBCO films: A micro-raman spectroscopy study. Doctoral thesis. (Universitat autonoma de Barcelona, Spain, 2005)

9. O. Castaño Linares, Síntesis y caracterización de capas delgadas superconductoras de altas corrientes críticas de $YBa_2Cu_3O_7$ obtenidas por MOD, Doctoral Thesis, (Universitat autonoma de Barcelona, Spain, 2004)

10. K.I. Itoh, A. Hashizume, H. Kohmoto, M. Matsuo, T. Endo, M. Mukaida, Magnetic anisotropy and vortex dynamics in a-oriented YBCO thin film characterized by microwave absorption. Physica C **357–360**, 477–480 (2001)

11. T. Araki, T. Yuasa, H. Kurosaki, Y. Yamada, I. Hirabayashi, T. Kato, T. Hirayama, Y. Lijima, T. Saito, High-J_c $YBa_2Cu_3O_{7-x}$ films on metal tapes by the metalorganic deposition method using trifluoroacetates. Supercond. Sci. technol. **15**, L1–L3 (2002)

12. J.M. Viña Rebolledo. Contribution to the study of the electric transport in cuprate superconducting thin films: supercritical currents and paraconductivity". PhD thesis. (University of Santiago de Compostela, Spain, 2003).

13. B. Ma et al., High critical current density of YBCO coated conductors fabricated by inclined substrate deposition. Physica C **403**, 183–190 (2004)

14. G. Majkic et al, Over 15 MA/cm^2 of critical current density in 4.8 μm thick, Zr-doped $(Gd,Y)Ba_2Cu_3O_x$ superconductor at 30 K, 3 T, Sci. Rep. **8**, 6982 (2018).

15. J. Du, S. Gnanarajan, A. Bendavid, Characterization of MgO substrates for growth of epitaxial YBCO thin films. Supercond. Sci. Technol. **18**, 1035–1041 (2005)

16. M. Chrobak et al. Thermal fluctuations in YBCO thin film on MgO substrate. Acta Phys. Pol. A. **126**, 88–91 (2014).

17. T. Nakamura et al, Transport characteristic in YBCO thin films under applying DC and AC currents. in *Advances in Superconductivity XI* by N. Koshizuka, S. Tajima. (Springer, Tokyo).

18. K. Matsumoto et al., High critical current density $YBa_2Cu_3O_{7-x}$ films on surface-oxidized metallic substrates. Physica C **335**, 39–43 (2000)

19. S.R. Foltyn et al., Strongly coupled critical current density values achieved in $YBa_2Cu_3O_{7-x}$ coated conductors with near-single-crystal texture. Appl. Phys. Lett. **82**, 4519 (2003)

20. B.H. Moeckly et al., Growth of $YBa_2Cu_3O_{7-x}$ thin films on MgO: The effect of substrates preparation. Appl. Phys. Lett. **57**, 1687 (1990)

21. M.I. Faley et al., Multilayer buffer for high-temperature superconductor devices on MgO. Appl. Phys. Lett **89**, 082507 (2006)

22. J.R. Groves et al., High critical current density $YBa_2Cu_3O_{7-x}$ thick films using ion beam assisted deposition MgO bi-axially oriented template layers on nickel-based superalloy substrates. J. Mater. Res. **16**, 2175 (2001)

23. B.D. Cullity, Elements of X-ray Diffraction" (Addison-Wesley Publishing Company, Inc. USA, 1956), pp.96-102.

24. J.I. Langford, A.J.C. Wilson, Scherrer after sixty years: a survey and some new results in the determination of crystallite size. J. Appl. Cryst. **11**, 102–113 (1978)

25. I. Hocas, R. Fernández, J.M. Gómez-Rodríguez, J. Colchero, J. Gómez-Herrero, A.M. Baro, WSXM: A software for scanning probe microscopy and a tool for nanotechnology. Rev. Sci. Instrum. **74**, 013705 (2007)

26. Powder Diffraction File PCPDFWIN, Version 2.1 JCPDS, The International Centre for Diffraction Data (2000).

27. B. Cappella, G. Dietler, Force-distance by atomic force microscopy. Surf. Sci. Rep. **34**, 1–104 (1999)

28. C.P. Bean, Magnetization of High-Field superconductors. Rev Mod. Phys. **36**, 31 (1964)

29. S. Eley, M. Miura, B. Maiorov, L. Civale, Universal lower limit on vortex creep in superconductors. Nat. Mater. **16**, 409–413 (2017)

30. R. Huhne et al., Coated conductor architectures based on IBAD-TiN for high-J_c YBCO films. Physica C **471**, 966–969 (2011)

31. I. Song et al., Shapiro-Steps in a YBCO Josephson junction array with inductive coupling lines. J. Korean Phys. Soc. **31**, 393–396 (1997)

32. J. Hudner et al., Thin-film growth and compositional effects in $YBa_2Cu_3O_{7-x}$ layers prepared by metalorganic chemical vapor deposition. J. Appl. Phys. **74**, 4631 (1993)